Jamming problems and the effects of compliance in dual peg-hole disassembly

Goli, Farzaneh; Zhang, Yongquan; Qu, Mo; Zang, Yue; Saadat, Mozafar; Pham, Duc truong; Wang, Yongjing

DOI:
10.1098/rspa.2023.0364

PROCEEDINGS A

royalsocietypublishing.org/journal/rspa

Research

Cite this article: Goli F, Zhang Y, Qu M, Zang Y, Saadat M, Pham DT, Wang Y. 2024 Jamming problems and the effects of compliance in dual peg-hole disassembly. *Proc. R. Soc. A* **480**: 20230364.
https://doi.org/10.1098/rspa.2023.0364

Received: 23 May 2023
Accepted: 14 February 2024

Subject Areas:
mechanical engineering

Keywords:
dual peg-hole extraction, disassembly, active compliance centre, robotic, force analysis, jamming

Author for correspondence:
Farzaneh Goli
e-mail: fxg174@student.bham.ac.uk

Jamming problems and the effects of compliance in dual peg-hole disassembly

Farzaneh Goli[1], Yongquan Zhang[2], Mo Qu[1], Yue Zang[1], Mozafar Saadat[1], Duc Truong Pham[1] and Yongjing Wang[1]

[1]Mechanical Engineering Department, University of Birmingham, Birmingham, UK
[2]Mechanical Engineering Department, Wuhan University of Technology, Wuhan, People's Republic of China

FG, 0009-0001-6304-3054; YZ, 0000-0003-4768-7279; MQ, 0000-0002-2333-4412; YZ, 0000-0002-1735-8880; MS, 0000-0002-6622-4715; DTP, 0000-0003-3148-2404; YW, 0000-0002-9640-0871

Disassembly is a crucial step in remanufacturing and is currently mainly performed by humans. Automating disassembly can reduce labour costs and make remanufacturing more economically attractive. This paper focuses on identifying and characterizing a common disassembly task, dual peg-hole disassembly, with the aim of building a robotic disassembly system for this task. We enumerate the possible contact states and their geometric conditions during the extraction of two studs in a dual peg-hole. This paper focuses on jamming in the extraction and conducts geometrical and quasi-static analyses to determine the boundary conditions of jamming. Based on the analyses, this paper also investigates the role of active compliance as a solution to avoid jamming. We also simulate critical variables and examine key parameters such as the degree of compliance, the location of the compliance centre and initial position errors. Finally, we conduct experimental studies on dual peg-hole extraction with different compliance centres obtained using active compliance.

THE ROYAL SOCIETY PUBLISHING

1. Introduction

The disposal of end-of-life (EOL) products presents a global challenge with a profound impact on both the environment and the economy [1]. To mitigate these impacts, EOL products are often recycled, reused, and remanufactured so that their components and materials can be separated non-destructively for future reuse [2].

Remanufacturing involves several stages, including disassembly, cleaning, inspection, repair or replacement of damaged parts, reassembly and testing [3]. Disassembly is a crucial step that links product return with product recovery [4]. However, manual disassembly can be inefficient. To reduce time and labour costs and improve efficiency, automatic disassembly using robotics can be employed [5]. One common task in disassembly is extracting a peg from a clearance-fit hole [6].

The extraction of a peg from a hole is a routine operation in the disassembly of mechanical components, such as detaching a shaft from a bearing in automotive turbochargers [7] and electric motors [8]. This procedure extends to the disassembly of assemblies with multiple peg-holes or dual peg-holes, as seen in examples such as electric plugs, capacitors and resistors.

While there have been many studies on peg-hole assembly, few studies have focused on disassembly. In the assembly and disassembly process, disassembly has received less attention. The geometry of assembly parts plays a key role in both processes. Lateral and angular misalignment between separated components can increase reaction forces and cause problems during disassembly. Unbalanced forces can cause jamming and wedging in disassembly, and this is a significant risk in the use of robots in peg-hole disassembly.

Jamming and wedging can occur due to reaction forces, preventing successful completion of the task and causing damage to the components and robotics [9]. Whitney analysed the quasi-static assembly of a cylindrical peg into a chamfered hole [10]. By using industrial robot strategies such as the remote compliance centre (RCC) [10–13], the jamming and wedging problem can be solved, allowing for successful insertion and extraction of pegs [11,12].

Simunovic [14] and Whitney [15] used a compliant manipulator to analyse peg-hole assembly and developed an RCC device to improve accuracy and efficiency. Researchers have also analysed rectangular peg insertion without chamfers [16] and three-dimensional rectangular peg insertion [17,18]. Sturges *et al.* also developed Spatial Remote Centre Compliance (SRCC) [19].

Strip [20] developed a hybrid force-position strategy for three-dimensional convex pegs using active compliance. Zhang *et al*. performed a quasi-static analysis of peg-hole disassembly with a compliance device, exploring the effect of key variables such as the degree of compliance, compliance centre location and position error [12]. Wang *et al*. compared passive and active compliance and found that active compliance was more beneficial due to its faster dynamic response [21]. Despite its cost and limited response speed, active compliance is an effective method for improving assembly reliability [22]. Sathirakul & Sturges [23] and Fei & Zhao [24] applied the compliance principle in multi peg-hole assembly tasks to correct lateral and angular misalignments. However, there has been a lack of in-depth investigation into multi-peg-hole disassembly. This has resulted in a knowledge gap regarding the mechanisms and contacts involved in the process.

In our previous studies [12,25], we explored contact states within one-peg and one-hole scenarios, characterized by limited contact points typically concentrated at the peg tip and hole's inner surface. These situations featured simpler geometries. In this paper, we delve into the intricacies of dual peg-hole scenarios, where each of the two pegs can establish numerous contact states with their respective holes. These contact points may manifest at various locations along the pegs, resulting in a more complex contact geometry compared to the one-peg-one-hole case. This research is motivated by the demand to address these complexities.

This paper shows an analysis of dual peg-hole extraction problems in two dimensions, highlighting the boundary conditions of jamming and proposing a solution using active compliance to avoid jamming.

The effectiveness of the active compliance strategy in robotics for peg-hole assembly and disassembly lies in its adaptability, precise force control [12], sensitivity, safety, efficiency,

versatility and demonstrated real-world applications. This approach empowers robots to dynamically adjust to their environment, responding in real time to factors such as misalignments or surface irregularities, thus reducing the length of the jamming area in peg-hole operations. Additionally, by employing force sensing, robots can accurately apply the necessary force for insertion and removal without causing damage to the components. This precision and adaptability make active compliance a valuable and reliable solution, particularly in industrial settings demanding high-precision performance [26].

Section 2 presents an analysis of multiple peg extraction during disassembly. Section 3 provides a geometric analysis of dual-peg extraction. Section 4 describes the force analysis of dual-peg extraction. Section 5 presents the experimental design and the results that confirm the theoretical disassembly model.

2. Analysis of multiple peg extraction during disassembly

Dual peg-hole extraction is a disassembly task in which two pegs are held together, moved together, and removed from their respective holes at the same time (figure 1). Although peg-hole disassembly is a three-dimensional problem, it can be schematically illustrated and analysed in two dimensions for simplicity [6]. To ensure that the simplified two-dimensional model can represent three-dimensional contact conditions, Lan *et al.* [25] investigated the correctness of using two- instead of three-dimensional models for peg-hole system analysis and compared the results obtained from two- and three-dimensional models. The authors concluded that the two-dimensional model can be used to represent the challenges in three dimensions if the following conditions are met:

1. The peg and hole are circular and axisymmetric.
2. The peg and hole are aligned.
3. The peg is not tilted.
4. The clearance between the peg and hole is smaller than the peg size.

Given these insights, we also adopted the simplified two-dimensional model for our analysis, which focuses on the geometry and contact states of dual peg-holes.

The analysis assumes two pegs of equal length and makes the following assumptions: (a) the pegs are stiff, (b) extraction occurs only vertically upwards and (c) the active compliance centre is located along the extraction axis between the two holes.

Based on the assumptions stated above, the forces and moments generated by contacts between pegs and holes can be calculated. Predicting force and torque during disassembly helps identify configurations in which the compliant devices supporting the pegs, such as a remote centre compliance (RCC), spatial RCC (SRCC) or active compliance centre, may fail to avoid wedging and jamming [23]. The force/torque analysis provides a better understanding of the physics of multiple peg-out-hole extractions using compliance mechanisms. The extraction phase of the dual-peg extraction problem is thoroughly examined in the following sections.

3. Geometric analysis of dual-peg extraction

(a) Extractability

Consider a dual peg-hole set with dimensions as shown in figure 1. Peg 1 and Peg 2 have radii of r_{P_1} and r_{P_2}, respectively. Hole 1 and Hole 2 have radii of R_{H_1} and R_{H_2}, respectively. The distance between the axes of the pegs is D_P, and the distance between the axes of the holes is D_H. The distance between Peg 1 and Hole 1 is C_1, and the distance between Peg 2 and Hole 2 is C_2. The current extraction depth is represented by h.

The necessary conditions for dual peg-hole disassembly are as follows:

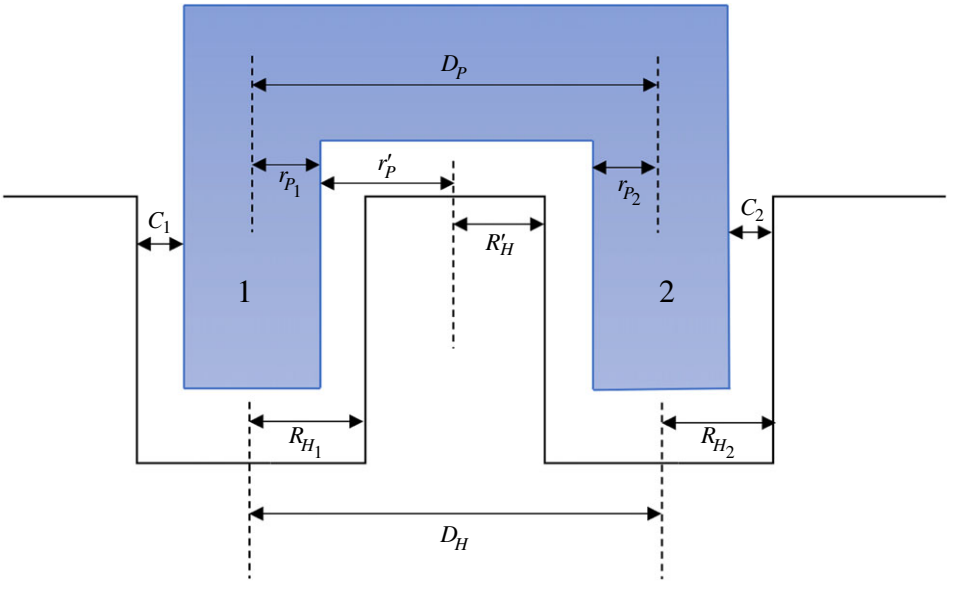

Figure 1. The geometric model of a dual peg-hole.

(a) The pegs must be smaller than their corresponding holes

$$r_{P_1} < R_{H_1} \quad \text{and} \quad r_{P_2} < R_{H_2}. \tag{3.1}$$

(b) The distance between the outer edges of the pegs must be less than the distance between the outer edges of the holes

$$D_P + r_{P_1} + r_{P_2} < D_H + R_{H_1} + R_{H_2}. \tag{3.2}$$

(c) The distance between the inner edges of the pegs must be greater than the distance between the inner edges of the holes

$$D_P - r_{P_1} - r_{P_2} > D_H - R_{H_1} - R_{H_2}. \tag{3.3}$$

Conditions b and c can be written as $-(C_1 + C_2) < D_H + D_P < C_1 + C_2$, where C_1 and C_2 are the clearances, e.g. $C_1 = R_{H_1} - r_{P_1}$ and $C_2 = R_{H_2} - r_{P_2}$. For the dual pegs to be extracted, all these conditions must be met at the same time. The ability of pegs to be extracted from their corresponding holes is referred to as extractability.

(b) Prediction of possible contact states

Figure 2 shows dual pegs that are extractable based on their maximum left and right travels. The pegs are rotated clockwise and anticlockwise while maintaining their current contact to produce other possible contact states. There are 13 possible contact states [23] that can exist in a dual peg-hole disassembly process (table 1). The contact states can be divided into four main groups: (a) no contact, (b) one-point contact, (c) two-point contact and (d) line contact, as shown in figure 3.

Ideally, the pegs should be in a state of no contact, but this rarely happens. The process typically begins with two-point contact due to compliant manipulation and the presence of lateral and angular errors. This occurs when a compliant manipulator grips a peg, causing it to shift and rotate (figure 3*c*). As the peg is extracted, the errors may decrease due to compliance, and the process may transfer to one-point contact (figure 3*b*) or line contact (figure 3*d*). To transfer from the two-point to one-point contact, the peg must rotate during the extraction process (figure 3*b*). The one-point contact state is maintained until the peg is completely extracted from the hole.

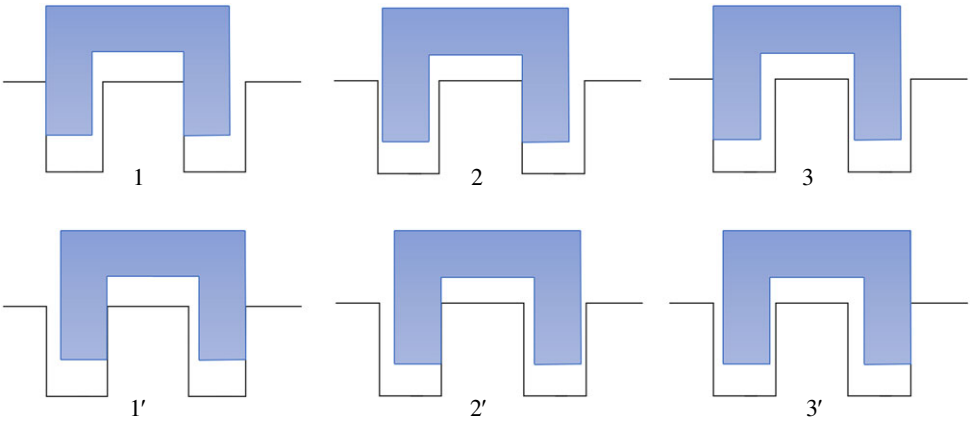

Figure 2. Maximum left- and right-side travel cases.

Table 1. Various contact states for dual-peg extractions.

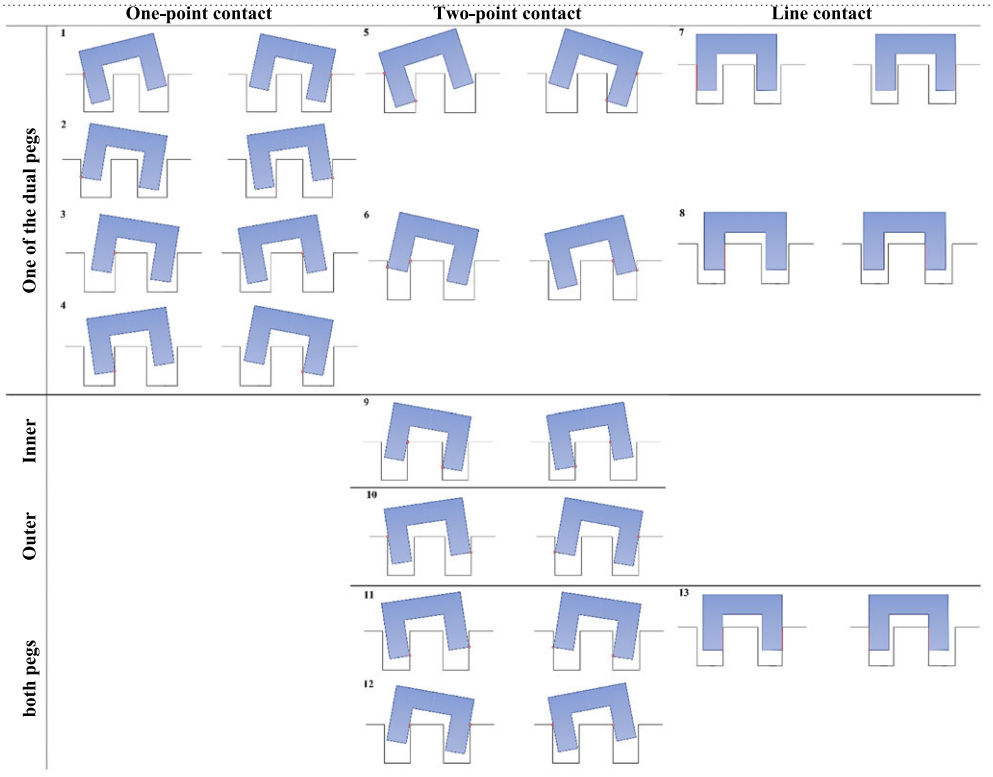

Sathirakul & Sturges [23] and Fei & Zhao [27] found that in two-dimensional cases, the three-point and four-point contact states during peg-in-hole insertion can only exist when certain conditions are met, such as given dimensions and associated insertion depth. As a result, these contact states are considered transient and unimportant in peg-hole insertion. Peg-hole insertion and extraction follow the same geometric analysis.

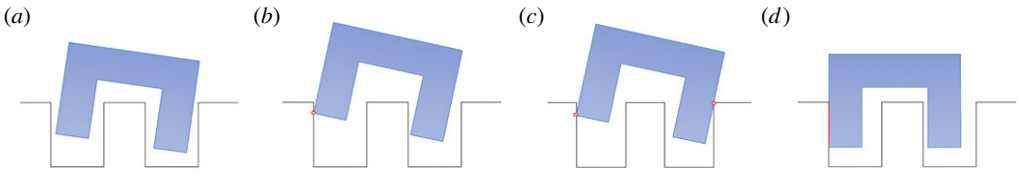

Figure 3. Typical states of the dual peg-hole disassembly process: (*a*) no contact, (*b*) one-point contact, (*c*) two-point contact and (*d*) line contact.

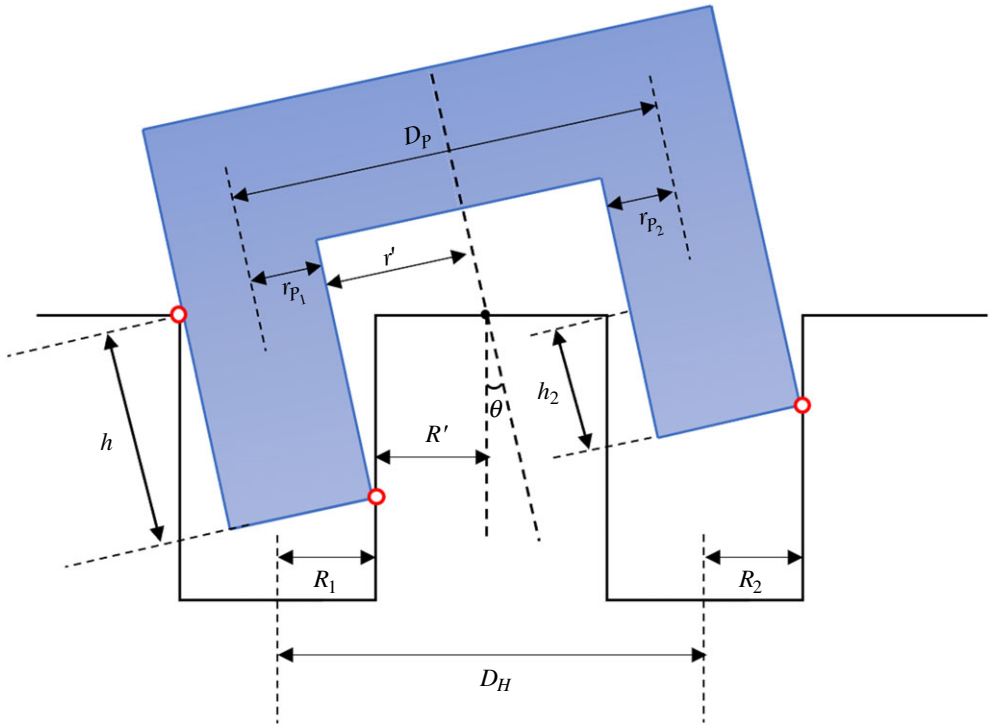

Figure 4. Three-point contact state of dual peg-in-hole.

A three-point contact can occur if equations (3.1) and (3.2) are satisfied simultaneously (θ is the tilt angle of the peg)

$$h\sin\theta + 2r_{P_1}\cos\theta = 2R_{H_1} \tag{3.1a}$$

and

$$h\sin\theta + (2r_{P_1} + 2r'_P + 2r_{P_2})\cos\theta = 2R_{H_1} + 2R'_H + 2R_{H_2}. \tag{3.2b}$$

Similarly, four-point contact can only occur if equations (3.1) and (3.3) are both satisfied (figure 4).

$$h_2\sin\theta + (2r_{P_2})\cos\theta = 2R_{H_2}. \tag{3.3c}$$

Therefore, three-point and four-point contacts are considered transitory and insignificant, as they only occur at specific insertion depth points rather than in a depth region [23,27].

Jamming is a common problem in peg-hole disassembly. Jamming occurs when a peg is unable to move due to improperly applied forces and moments. It can occur in the two-point contact state and can be avoided by reducing the two-point contact region and controlling the position where two-point contact occurs [28]. In the case of three-point and four-point contacts, these issues are

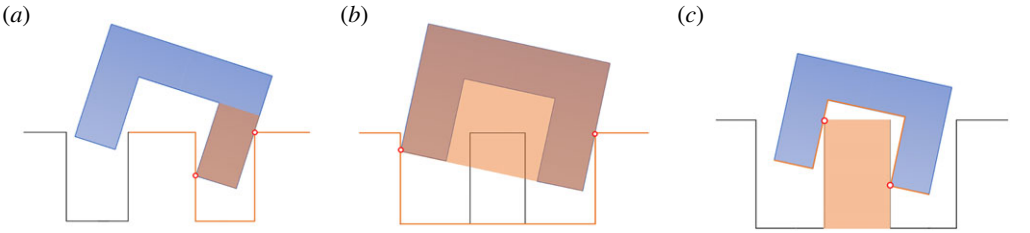

Figure 5. Classification of two-point contact states in dual peg-hole disassembly.

minimal because they occur at specific depth points rather than at specific regions. As a result, this study focuses on jamming analysis in two-point contact states.

4. Force analysis of dual-peg extraction

Analysing forces and moments during dual-peg extraction is important for planning fine motions. Several conditions must be met for successful extraction of dual pegs from their holes. During extraction, the dual pegs may experience various contact states, some of which may be more desirable than others. To maintain each contact state, it is necessary to derive the conditions of applied forces and moments. A two-dimensional dual-peg problem may have 13 possible states (table 1), but contact states with more than two-point contacts are insignificant in jamming, as explained in §3. In general, dual peg-hole problems can be considered similar to one peg-hole problem in terms of two-point contact states (figure 5). Two-point contact states in dual peg-holes can be categorized into three groups: (a) contact in one of the dual peg-holes, (b) external surfaces of pegs contacting hole surfaces and (c) inner surfaces of pegs contacting hole surfaces. This section analyses a contact from each category.

(a) Derivation of force–moment conditions for maintaining contact states

Consider two pegs of the same length with dimensions, as shown in figure 6*a*. The reference frame for the dual pegs in each state is located at the end of the selected peg (shown in orange). All forces and moments acting on the pegs are prescribed with respect to this reference frame. It is assumed that the dual pegs and the hole are initially in two-point contact and that the angle is small to simplify the calculations. This assumption is valid because, in practice, the peg's angular error is typically only a few degrees at most.

As shown in figure 6*b*, δ_0 and β_0 represent the initial lateral and angular errors, respectively. The compliance centre and the tip of the peg are located at distances U_0 and ε_0 from the axis of the hole, respectively.

(i) Contact in one of the dual peg-holes

In this section, the contact states of two points that occur in one of the peg-holes (figure 5*a*) are analysed. There are four possible contact states in this situation. The force analysis of one of these contact states is presented here as an example. Consider the quasi-static equilibrium condition of double pegs in contact mode 5 (table 1), as shown in figure 7. Extraction forces (F_z), (F_x) and moments (M) are applied to the studs at point O, which is the origin of the reference frame. The distances U and ε vary continuously during disassembly. The path of the compliance centre can be deduced as follows:

$$\left.\begin{aligned} U+\varepsilon &= L_{\mathrm{C}}\sin\theta,\\ U-U_0+(\varepsilon-\varepsilon_0) &= L_{\mathrm{C}}(\theta-\theta_0)\\ \varepsilon &= r'\cos\theta - R' \end{aligned}\right\} \quad (4.1)$$

and

$$U-U_0 = L_{\mathrm{C}}(\theta-\theta_0).$$

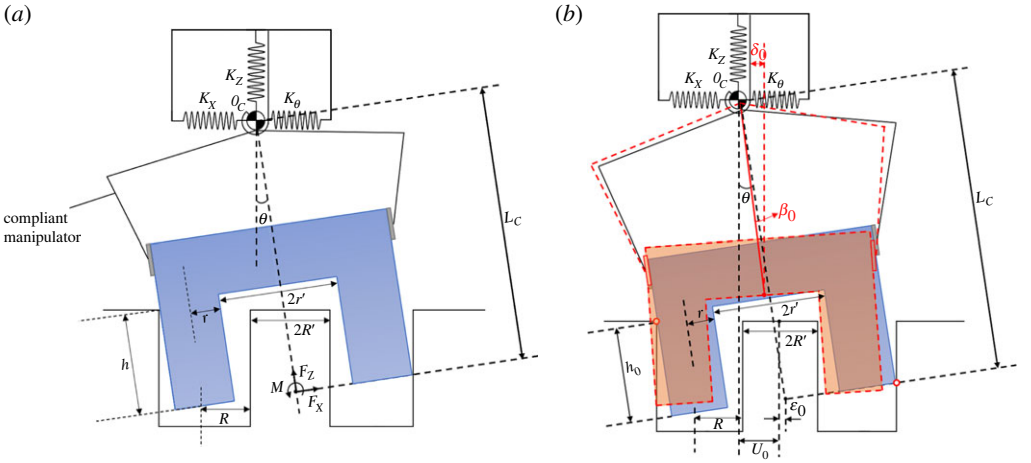

Figure 6. (*a*) Dimensions and reference frame for dual peg-hole. (*b*) Definition of the initial position in the dual peg-hole.

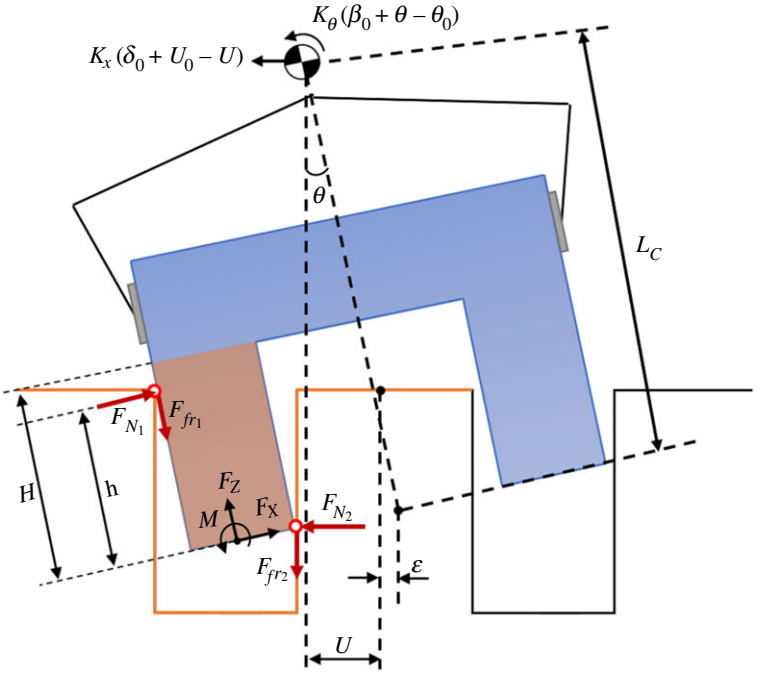

Figure 7. Geometry and forces during the two-point contact in one of the dual peg-holes.

In this equation, L_C is the distance between the compliance centre and tip of the pegs, and h is the depth of peg extraction.

During two-point contact, the geometrical relations are as follows, based on geometrical constraints between the dual peg-holes

$$R = \frac{h \sin\theta}{2} + r\cos\theta. \tag{4.2}$$

In the case of small clearances between pegs and holes, equation (4.2) can be simplified as

$$h\theta = 2\complement R, \quad \complement = \frac{R-r}{R}; \quad \complement : \text{Clearance ratio for first peg-hole.} \tag{4.3}$$

Whitney's [10] method can be re-expressed contact and supporting forces at and around the compliance centre in the coordinate frame fixed at the tip of the selected peg.

$$\left.\begin{aligned} F_x &= F_{N2} - F_{N1}, \\ F_z &= \mu(F_{N1} + F_{N2}) \\ \text{and} \quad M &= (h-\mu r)F_{N1} + \mu r F_{N2}. \end{aligned}\right\} \tag{4.4}$$

The following is the applied force and moment by compliance centre:

$$\left.\begin{aligned} F_x &= -K_x(\delta_0 + U_0 - U) \\ \text{and} \quad M &= K_x L_\complement(\delta_0 + U_0 - U) + K_\theta(\beta_0 + \theta - \theta_0). \end{aligned}\right\} \tag{4.5}$$

By assuming $F_{N2} = 0$ for the contact force at point 2, it is possible to calculate the boundary conditions for the two-point contact. Accordingly, the contact forces are as follows:

$$\left.\begin{aligned} F_x &= -F_{N1} \\ F_z &= \mu F_{N1} \\ \text{and} \quad M &= (h-\mu r)F_{N1}. \end{aligned}\right\} \tag{4.6}$$

The path of the centre of compliance in the boundary conditions of the two-point contact state is expressed as follows using equations (4.1) and (4.6):

$$\left.\begin{aligned} \theta &= \theta_0 - \beta_0 + \frac{K_x(h-\mu r - L_\complement)(L_\complement\beta_0 + \delta_0)}{K_x L_\complement(h-\mu r) - K_x L_\complement^2 + K_\theta} \\ \text{and} \quad U &= U_0 + \delta_0 - \frac{K_\theta(L_\complement\beta_0 + \delta_0)}{K_x L_\complement(h-\mu r) - K_x L_\complement^2 + K_\theta}. \end{aligned}\right\} \tag{4.7}$$

By substituting equations (4.2) and (4.3) into equation (4.7), a quadratic equation can be generated, which will be the roots of the equation for extraction depth h

$$\alpha h^2 + \beta h + \gamma = 0, \tag{4.8}$$

where

$$\alpha = A + K_x L_\complement B,$$

$$\beta = (E - \mu r K_x L_\complement)B - (L_\complement + \mu r)A - 2cRK_x L_\complement,$$

$$\gamma = 2cR(\mu r K_x L_\complement - E),$$

$$A = K_x(L_\complement\beta_0 + \delta_0),$$

$$B = \theta_0 - \beta_0$$

and

$$E = K_\theta - K_x L_\complement^2.$$

The roots (extraction depth[1]) of equation (4.8) are

$$h_2 = \frac{-\beta + \sqrt{\beta^2 - 4\alpha\gamma}}{2\alpha}, h_2' = \frac{-\beta - \sqrt{\beta^2 - 4\alpha\gamma}}{2\alpha}. \tag{4.9}$$

The roots h_2 and h_2', which represent the beginning and end of a two-point contact zone, can be found by solving equation (4.8).

[1]The period of the equation's roots (h_2 and h_2') is discussed in section 4a(iv).

In the one-point contact state, the geometrical parameters are as follows ($\theta \approx 0$):

$$\left.\begin{aligned} U &= L_C\theta - \varepsilon, \\ \varepsilon &= r'\cos\theta - R' \\ \text{and} \quad U &= L_C\theta - r' + R'. \end{aligned}\right\} \tag{4.10}$$

The equations for U and θ and of the one-point contact can be obtained by combining equations (4.5) and (4.6) in a coordinate frame fixed to the selected peg tip.

$$\left.\begin{aligned} U &= \delta_0 + U_0 - \frac{N_2 + K_\theta\theta}{K_x(h - \mu r - L_C)} \\ \text{and} \quad \theta &= \frac{N_2 - K_x N_1(h - \mu r - L_C)}{-K_x L_C(h - \mu r - L_C) - K_\theta}, \end{aligned}\right\} \tag{4.11}$$

where

$$\begin{aligned} N_1 &= \delta_0 + U_0 - R' + r' \\ \text{and} \quad N_2 &= K_\theta(\beta_0 - \theta_0). \end{aligned} \tag{4.12}$$

The reaction force and extraction force during the two-point contact can be obtained from equation (4.4), which is composed of three equations and three unknown parameters

$$\left.\begin{aligned} F_{N1} &= -\frac{\mu r}{h}F_x + \frac{1}{h}M, \\ F_{N2} &= \frac{h - \mu r}{h}F_x + \frac{1}{h}M \\ \text{and} \quad F_z &= \frac{M}{\lambda r} - \frac{\mu}{\lambda}(1 - \lambda)F_x; \quad \lambda = \frac{h}{2r\mu}. \end{aligned}\right\} \tag{4.13}$$

Equation (4.5) with equations (4.1) and (4.3) substituted produces F_x and M for the two-point contact state.

$$\left.\begin{aligned} F_x &= -k_x\left(\delta_0 + L_C\theta_0 - \frac{cDL_C}{h}\right) \\ \text{and} \quad M &= k_x L_C(\delta_0 + L_C\theta_0) - \frac{k_x {L_C}^2 CD}{h} + k_\theta(\beta_0 - \theta_0) + \frac{k_\theta CD}{h}, \end{aligned}\right\} \tag{4.14}$$

where $h\theta = 2CR = CD; D = 2R$.

By substituting equation (4.11) into equation (4.6), the extraction force in the one-point contact state is calculated.

$$F_z = \frac{\mu k_\theta(\theta - \theta_0 + \beta_0)}{(h - \mu r - L_C)}. \tag{4.15}$$

(ii) External surfaces of pegs contacting hole surfaces

In this part, the states where the external surfaces of the pegs contact the hole surfaces are analysed, as shown in figure 5*b*. There are four possible contact states in this situation, and one of these contact states is presented as an example. Consider the quasi-static equilibrium condition in contact mode 10, as shown in table 1. Extraction forces, F_X and F_z, and moments, M, are applied to the stud at point O, which is the origin of the reference frame. The distances U and ε (figure 8) are very continuous during disassembly.

where in this case, $2R = 2R_{H_1} + 2R_{H_2} + 2R'$and $2r = 2r_{p_1} + 2r_{p_2} + 2r'$.

The path of the compliance centre can be deduced as follows:

$$\left.\begin{aligned} U + \varepsilon &= L_C\sin\theta; \varepsilon = \frac{h\theta}{2} \\ \text{and} \quad U - U_0 + \left(\tfrac{h\theta}{2} - \varepsilon_0\right) &= L_C(\theta - \theta_0). \end{aligned}\right\} \tag{4.16}$$

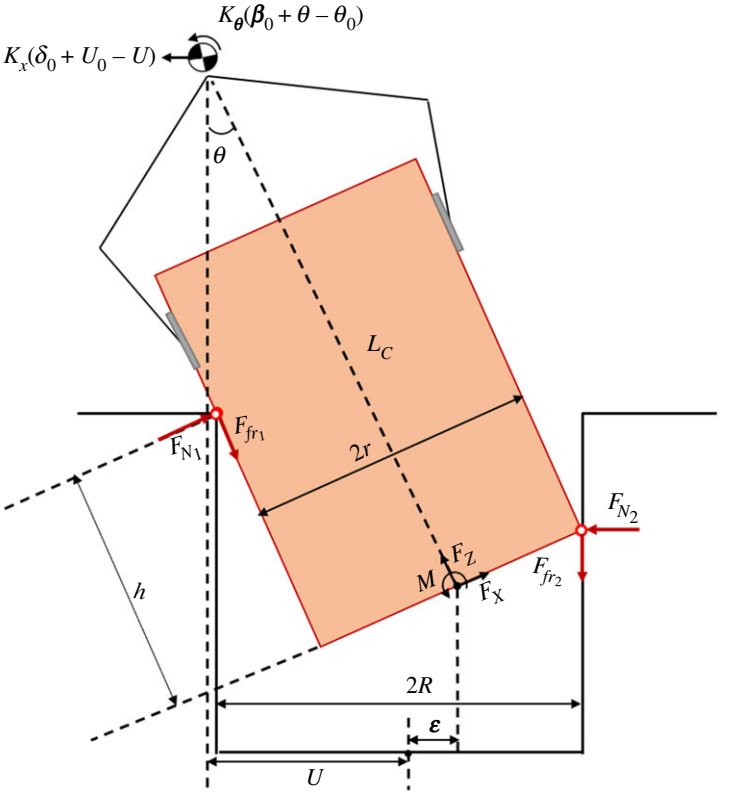

Figure 8. Geometry and forces during the two-point contact in the external surfaces of pegs contact holes surfaces.

During two-point contact, the geometrical relations are as follows, based on geometrical constraints between the dual peg-holes

$$R = \left(\frac{h}{2}\right)\sin\theta + r\cos\theta. \tag{4.17}$$

In the case of small clearances between pegs and holes, equation (4.17) can be simplified as

$$h\theta = 2\mathbb{C}R; \quad \mathbb{C} = \frac{(R-r)}{R}; \quad \mathbb{C}: \text{clearance ratio for both peg-hole.} \tag{4.18}$$

Contact forces and supporting forces at and about the compliance centre in the coordinate frame fixed at the tip of the peg

$$\left.\begin{aligned} F_x &= F_{N2} - F_{N1}, \\ F_z &= \mu(F_{N1} + F_{N2}) \\ \text{and} \quad M &= (h-\mu r)F_{N1} + \mu r F_{N2}. \end{aligned}\right\} \tag{4.19}$$

The following is the applied force and moment by compliance centre:

$$\left.\begin{aligned} F_x &= -K_x(\delta_0 + U_0 - U) \\ \text{and} \quad M &= K_x L_{\mathbb{C}}(\delta_0 + U_0 - U) + K_\theta(\beta_0 + \theta - \theta_0). \end{aligned}\right\} \tag{4.20}$$

Boundary conditions of two-point contact when $F_{N2} = 0$:

$$\left.\begin{aligned} F_x &= -F_{N1}, \\ F_z &= \mu F_{N1} \\ \text{and} \quad M &= (h-\mu r)F_{N1}. \end{aligned}\right\} \tag{4.21}$$

The path of the compliance centre in the boundary conditions of the two-point contact state is expressed as follows using equations (4.16) and (4.21):

$$\left.\begin{aligned}\theta &= \theta_0 - \beta_0 + \frac{K_x(h-\mu r-L_C)(L_C\beta_0+\delta_0+CR-\varepsilon_0)}{K_xL_C(h-\mu r)-K_xL_C^2+K_\theta}\\ \text{and}\quad U &= U_0+\delta_0-\frac{K_\theta(L_C\beta_0+\delta_0+CR-\varepsilon_0)}{K_xL_C(h-\mu r)-K_xL_C^2+K_\theta}.\end{aligned}\right\} \tag{4.22}$$

A quadratic equation can be generated by substituting equations (4.17) and (4.18) into equation (4.22), which will be the roots of the equation for extraction depth[2] h

$$\alpha h^2+\beta h+\gamma=0, \tag{4.23}$$

where

$$\begin{aligned}\alpha &= A+K_xL_CB,\\ \beta &= (E-\mu rK_xL_C)B-(L_C+\mu r)A-2cRK_xL_C,\\ \gamma &= 2CR(\mu rK_xL_C-E),\\ A &= K_x(L_C\beta_0+\delta_0+CR-\varepsilon_0),\\ B &= \theta_0-\beta_0\\ E &= K_\theta-K_xL_C^2.\end{aligned}$$

The solutions of equation (4.23)

$$h_2=\frac{-\beta+\sqrt{\beta^2-4\alpha\gamma}}{2\alpha},\quad h_2'=\frac{-\beta-\sqrt{\beta^2-4\alpha\gamma}}{2\alpha}. \tag{4.24}$$

The geometrical constraints during one-point contact ($\theta\approx 0$)

$$U=L_C\theta-h\theta+CR. \tag{4.25}$$

The path of the compliance centre during one-point contact by using equations (4.20) and (4.21)

$$\left.\begin{aligned}U &= \delta_0+U_0-\frac{N_2+K_\theta\theta}{K_x(h-\mu r-L_C)}\\ \text{and}\quad \theta &= \frac{N_2-K_xN_1(h-\mu r-L_C)}{-K_x(L_C-h)(h-\mu r-L_C)-K_\theta},\end{aligned}\right\} \tag{4.26}$$

where

$$\left.\begin{aligned}N_1 &= \delta_0+U_0-CR\\ \text{and}\quad N_2 &= K_\theta(\beta_0-\theta_0).\end{aligned}\right\} \tag{4.27}$$

The reaction force and extraction force during the two-point contact can be obtained from equation (4.19)

$$\left.\begin{aligned}F_{N1} &= -\frac{\mu r}{h}F_x+\frac{1}{h}M,\\ F_{N2} &= \frac{h-\mu r}{h}F_x+\frac{1}{h}M\\ \text{and}\quad F_z &= \frac{M}{\lambda r}-\frac{\mu}{\lambda}(1-\lambda)F_x;\quad \lambda=\frac{h}{2r\mu}.\end{aligned}\right\} \tag{4.28}$$

F_x and M for two-point contact by using equations (4.16), (4.18) and (4.20)

$$\left.\begin{aligned}F_x &= -k_x\left(\delta_0-\varepsilon_0+L_C\theta_0+\frac{CD}{2}-\frac{cDL_C}{h}\right)\\ \text{and}\quad M &= k_xL_C\left(\delta_0-\varepsilon_0+L_C\theta_0+\frac{CD}{2}\right)-\frac{k_xL_C^2CD}{h}+k_\theta(\beta_0-\theta_0)+\frac{k_\theta CD}{h}.\end{aligned}\right\} \tag{4.29}$$

[2]The period of the equation's roots (h_2 and h_2') is discussed in section 4a(iv).

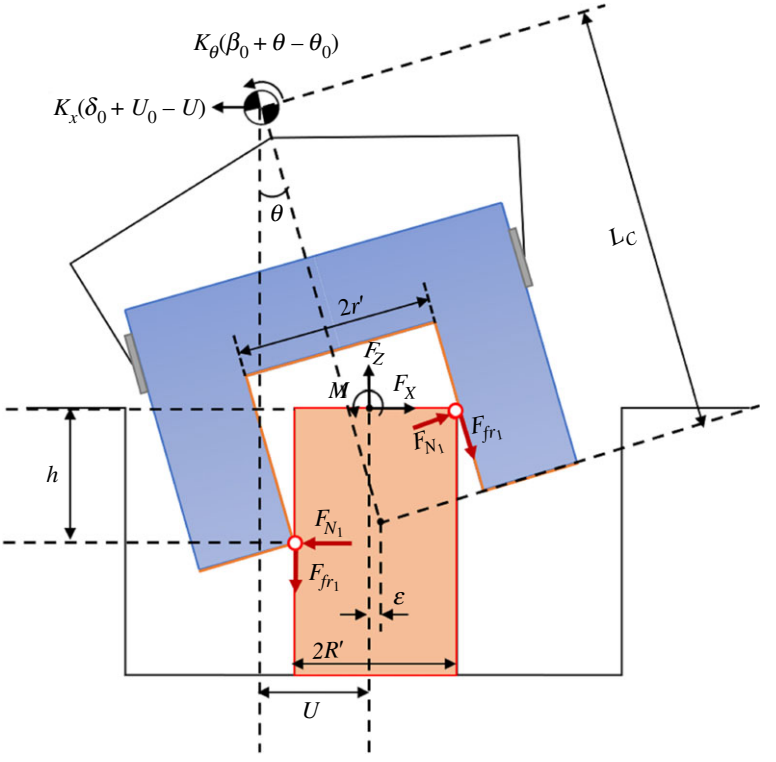

Figure 9. Geometry and forces during two-point contact in the inner surfaces of pegs contact hole surfaces.

The extraction force in the one-point contact state is calculated by substituting equation (4.26) into equation (4.21).

$$F_z = \frac{\mu k_\theta(\theta - \theta_0 + \beta_0)}{(h - \mu r - L_C)}. \tag{4.30}$$

(iii) Inner surfaces of pegs contacting holes' surfaces

This section analyses the two-point contact state where the inner surfaces of pegs contact holes. As shown in figure 5*c*, an inverted peg-hole is considered. There are two possible contact states in this situation. As in the previous sections, the force analysis of one of these contact states is presented as an example. Consider the quasi-static equilibrium condition of the dual pegs in contact mode 9, as shown in table 1. The distances U and ε (figure 9) are very continuous during disassembly. The path of the compliance centre can be deduced as follows:

$$\left.\begin{aligned} U + \varepsilon &= L_C \sin\theta \\ \varepsilon &= r' \cos\theta - R' \\ \text{and} \quad U - U_0 &= L_C(\theta - \theta_0). \end{aligned}\right\} \tag{4.31}$$

Considering an inverted peg-hole, the radius of the hole, which is considered in this section as the radius of the peg, is as follows:

$$R' = \frac{r'}{\cos\theta} - \frac{h}{2}\tan\theta. \tag{4.32}$$

For small clearances between pegs and holes, equation (4.32) can be simplified as follows:

$$h\theta = 2R'C; \quad C = \frac{(R' - r')}{R}; \quad C: \text{clearance ratio for both peg-hole} \tag{4.33}$$

Contact forces and supporting forces at and about the compliance centre in the coordinate frame fixed at the tip of the peg are given by

$$\left.\begin{aligned} F_x &= F_{N2} - F_{N1}, \\ F_z &= \mu(F_{N1} + F_{N2}) \end{aligned}\right\} \tag{4.34}$$

and

$$\left.\begin{aligned} M &= (h - \mu R')F_{N1} + \mu R' F_{N2}. \end{aligned}\right\}$$

The following is the applied force and moment by compliance centre:

$$\left.\begin{aligned} F_x &= -K_x(\delta_0 + U_0 - U) \\ M &= K_x(L_C - h)(\delta_0 + U_0 - U) + K_\theta(\beta_0 + \theta - \theta_0). \end{aligned}\right\} \tag{4.35}$$

and

Boundary conditions of two-point contact when $F_{N1} = 0$

$$\left.\begin{aligned} F_x &= F_{N2}, \\ F_z &= \mu F_{N2} \end{aligned}\right\} \tag{4.36}$$

and

$$\left.\begin{aligned} M &= \mu R' F_{N2}. \end{aligned}\right\}$$

The path of the compliance centre in the boundary conditions of the two-point contact state is expressed as follows using equations (4.31), (4.35) and (4.36):

$$\left.\begin{aligned} \theta &= \theta_0 - \beta_0 + \frac{K_x(h - \mu R' - L_C)(\delta_0 + L_C\beta_0)}{K_x L_C(h - \mu R') - K_x {L_C}^2 + K_\theta} \\ U &= U_0 + \delta_0 - \frac{K_\theta(L_C\beta_0 + \delta_0)}{K_x L_C(h - \mu R') - K_x {L_C}^2 + K_\theta}. \end{aligned}\right\} \tag{4.37}$$

and

A quadratic equation can be generated by substituting equations (4.32) and (4.33) into equation (4.37), which will be the roots of the equation for extraction depth[3] h

$$\alpha h^2 + \beta h + \gamma = 0, \tag{4.38}$$

where

$$\alpha = A + K_x L_C B,$$

$$\beta = (E - K_x L_C^2)B - (\mu R' + L_C)A - (-2R'C)K_x L_C,$$

$$\gamma = (-2R'C)(K_x L_C^2 - E),$$

$$A = K_x(\delta_0 + L_C\beta_0),$$

$$B = \theta_0 - \beta_0$$

and

$$E = K_\theta - \mu R' K_x L_C.$$

So,

$$(A + K_x L_C B)h^2 + ((E - K_x L_C^2)B - (\mu R' + L_C)A - (-2R'C)K_x L_C)h + (-2R'C)(K_x L_C^2 - E) = 0.$$

The solutions of equation (4.38)

$$h_2 = \frac{-\beta + \sqrt{\beta^2 - 4\alpha\gamma}}{2\alpha}, \quad h_2' = \frac{-\beta - \sqrt{\beta^2 - 4\alpha\gamma}}{2\alpha}. \tag{4.39}$$

The geometrical constraints during one-point contact ($\theta \approx 0$)

$$\left.\begin{aligned} U &= L_C\theta - \varepsilon \\ \varepsilon &= r' - R' \end{aligned}\right\} \tag{4.40}$$

and

$$\left.\begin{aligned} U &= L_C\theta - r' + R'. \end{aligned}\right\}$$

[3]The period of the equation's roots (h_2 and h_2') is discussed in section 4a(iv).

The path of the compliance centre during one-point contact by using equations (4.35) and (4.36) and θ is obtained using equations (4.40) and U

$$\left.\begin{aligned} U &= \delta_0 + U_0 - \frac{N_2 + K_\theta\theta}{K_x(h - \mu R' - L_C)} \\ \text{and} \qquad \theta &= \frac{N_2 - K_x N_1(h - \mu R' - L_C)}{-K_x L_C(h - \mu R' - L_C) - K_\theta}, \end{aligned}\right\} \tag{4.41}$$

where

$$N_1 = \delta_0 + U_0 - R' + r', N_2 = K_\theta(\beta_0 - \theta_0). \tag{4.42}$$

The reaction force and extraction force during the two-point contact can be obtained from equation (4.34)

$$\left.\begin{aligned} F_{N1} &= -\frac{\mu R'}{h}F_x + \frac{1}{h}M \\ F_{N2} &= \frac{h - \mu R'}{h}F_x + \frac{1}{h}M \\ \text{and} \qquad F_z &= \frac{M}{\lambda R'} - \frac{\mu}{\lambda}(1 - \lambda)F_x; \quad \lambda = \frac{h}{2R'\mu}. \end{aligned}\right\} \tag{4.43}$$

F_x and M for two-point contact by using equations (4.31), (4.33) and (4.35)

$$\left.\begin{aligned} F_x &= -k_x\left(\delta_0 + L_C\theta_0 - \frac{L_C(-2R'C)}{h}\right) \\ \text{and} \qquad M &= k_x L_C(\delta_0 + L_C\theta_0 - h\theta - 2R'C) - \frac{k_x {L_C}^2(-2R'C)}{h} - k_x h\delta_0 + k_\theta(\beta_0 - \theta_0) + \frac{k_\theta(-2R'C)}{h}. \end{aligned}\right\} \tag{4.44}$$

The extraction force in the one-point contact state is calculated by substituting equation (4.41) into equation (4.36)

$$F_z = \frac{-\mu k_\theta(\theta - \theta_0 + \beta_0)}{(h - \mu R' - L_C)}. \tag{4.45}$$

(iv) Region of extraction depth

In equations (4.8), (4.23) and (4.38), h_2 and $h_2'^{'}$ are the two roots representing the depth of extraction (h). The parameters h_2 and h_2' represent the beginning and end of the two-point contact region, respectively. If $h_2' < h_0$ the peg and hole would be in the two-point contact area at the start of the disassembly process. If $h_0 < h_2' < h_2$, the peg-hole is initially in one-point contact, and there is at least one transformation between the one-point contact and two-point contact states. Two-point contact cannot occur during disassembly if the equations have no solution. If $h_0 < h_2' = h_2$, the peg-hole has a two-point contact state at a certain depth point. The height and position of the two-point contact region are influenced by many parameters, including the geometrical parameters of the hole-peg system, the location of the compliance centre, initial position errors and the degree of compliance.

(v) Jamming region

Jamming can be determined using equilibrium equations for rigid pegs [10]. Combining equations (4.4), (4.19) or (4.34) reveals the linear relationship for a peg in two-point contact

$$\frac{M}{hF_Z} = \frac{h}{2r\mu} - \frac{F_X}{F_Z}\left(\frac{h}{2r} - \mu\right) \tag{4.46}$$

and

$$\frac{F_X}{F_Z} = \pm\frac{1}{\mu}. \tag{4.47}$$

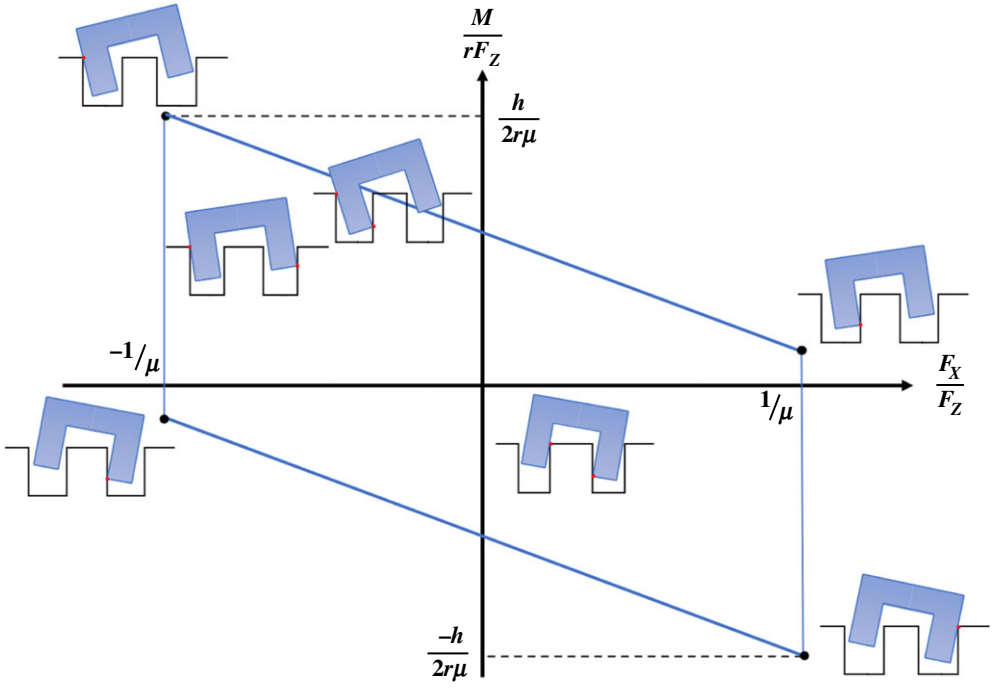

Figure 10. Jamming diagrams for the dual-peg extraction problem based on contact forces [23].

Based on (4.46) and (4.47),

$$\frac{M}{hF_Z} = \pm\left(\frac{h}{2r\mu} + 1\right). \tag{4.48}$$

As illustrated in figure 10, equations (4.46) and (4.48) define the equilibrium instance (shown by the outline of the parallelogram) where the pegs are extracted from the holes based on the combination of F_X, F_Z and M. Jamming occurs when combinations of F_X, F_Z and M fall outside the parallelogram, while successful extraction occurs when they fall within the parallelogram. As h decreases, the peg is closer to the mouths of the hole, and the probability of jamming decreases [11]. Jamming becomes less likely as the peg is extracted from the hole.

(b) Key factors and their effects

In the two-point contact state, the reaction forces applied to the pegs increase the risk of extraction failure, especially at the mouth of the hole. Two-point contact also increases the extraction force due to angular and lateral errors. This section identifies the most influential parameters for reducing the two-point region and their effect on its location.

Parameters L_C, δ_0, K_x and k_θ have been examined to demonstrate their impacts on the two-point contact region. These investigations are discussed in the following sections.

(i) Location of compliance centre

A key design parameter is the placement of the compliance centre along the central axis of the pegs. When a compliant manipulator grasps a peg, initial position errors between the manipulator and the dual peg-hole system cause the peg to shift and rotate. Assuming that the dual peg-hole is solid (figure 6*b*), the black figure shows the initial location of the peg before the initial angular error. However, the initial lateral error causes the peg to displace and rotate around the compliance centre (red figure). If the compliance centre is positioned far from the peg tip, the peg rotates anticlockwise around it. In this case, the one-point contact state might change into

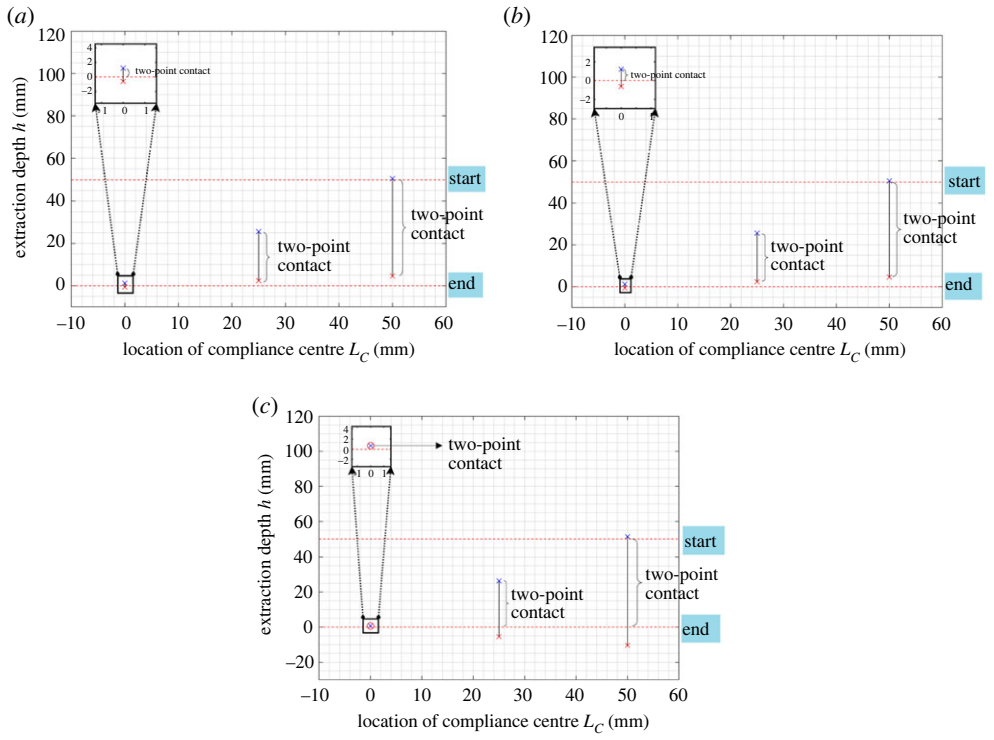

Figure 11. Dependence of the two-point contact region on the location of the compliance centre with $\delta_0 = 2$ mm, $\beta_0 = 0$ rad, $K_\theta = 4$ N mm^{-1}, $K_\theta = 30$ Nmm rad^{-1}. (*a*) Contact in one of the dual peg-holes, (*b*) External surfaces of pegs contact hole surfaces, (*c*) Inner surfaces of pegs contact hole surfaces.

a two-point contact. If the compliance centre is positioned at the peg tip, it rotates clockwise around it when grasped, resulting in one-point or line contact between the pegs and holes. These characteristics can help minimize the two-point contact region during disassembly. Figure 11 shows the boundary conditions of the two-point contact region based on the equations of extraction depth (h_2 and h_2'). It is clear that when the compliance centre is near the tip of the peg, the two-point contact area is significantly smaller. Additionally, as L_C decreases, the two-point contact region shifts to the hole mouth.

(ii) Initial position errors

The two-point contact region can be influenced by initial position errors, including lateral and angular errors between the compliant manipulator and the peg-hole system. When the compliance centre is located far from the tip, a large lateral δ_0 error can cause the peg to rotate anticlockwise significantly. If δ_0 is large enough, the peg and hole will remain in two-point contact during disassembly. If the compliance centre is at the tip, the peg rotates clockwise during disassembly. From the two-point contact, the hole and peg transition to one-point contact or line contact [12]. Figures 12–14 show the effects of the initial lateral error on the two-point contact region for various compliance centre locations. The two-point contact region decreases as the lateral error increases when the compliance centre is near the tip of the peg. Angle errors affect the disassembly process both in magnitude and direction. When the compliance centre is far from the peg tip and the initial angular error is opposite to the rotation of the peg, as shown in figure 15, a two-point contact region can be reduced. Otherwise, the two-point contact region increases. The effects of the initial angular error are similar when the compliance centre is at the tip of the peg.

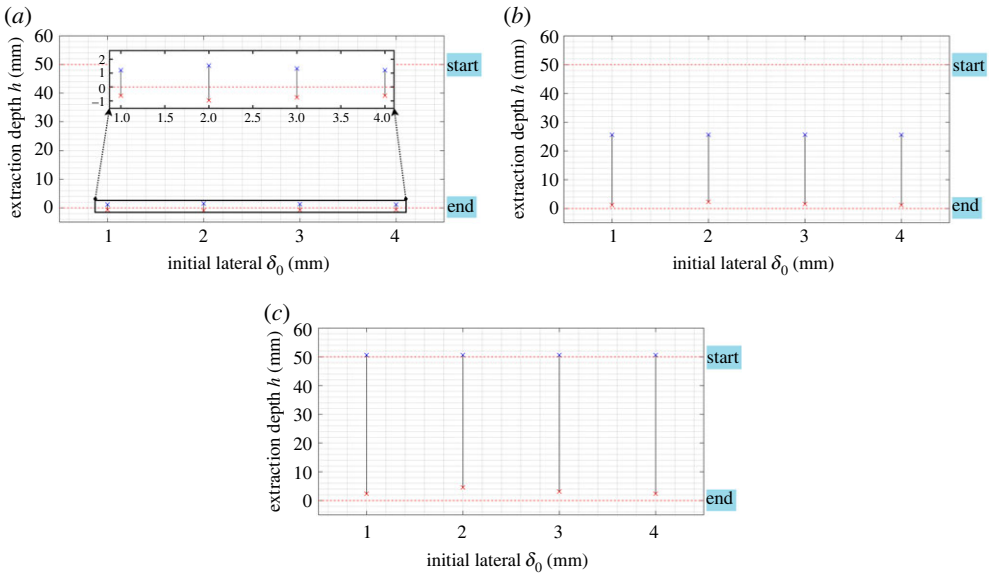

Figure 12. The effect of the initial lateral error on the two-point contact region in one of the dual peg-holes: (*a*) $L_C = 0$, (*b*) $L_C = 25$, (*c*) $L_C = 50$ with $\beta_0 = 0$ rad, $K_\Theta = 4$ N mm^{-1}, $K_\Theta = 30$ Nmm rad^{-1}.

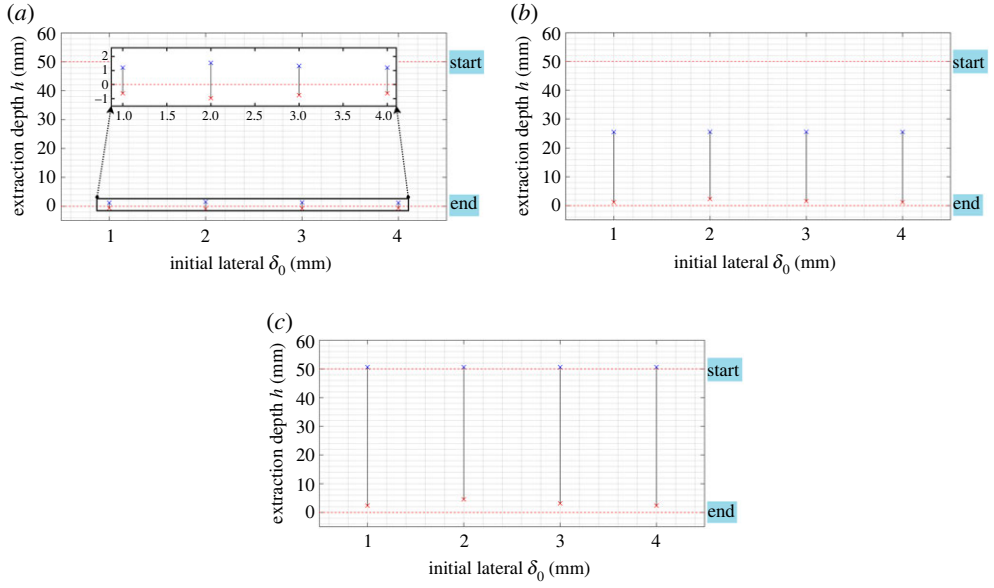

Figure 13. The effect of initial lateral error on the two-point contact region in the contact of the inner surfaces of the pegs with the holes: (*a*) $L_C = 0$, (*b*) $L_C = 25$, (*c*) $L_C = 50$ with $\beta_0 = 0$ rad, $K_\theta = 4$ N mm^{-1}, $K_\theta = 30$ Nmm rad^{-1}.

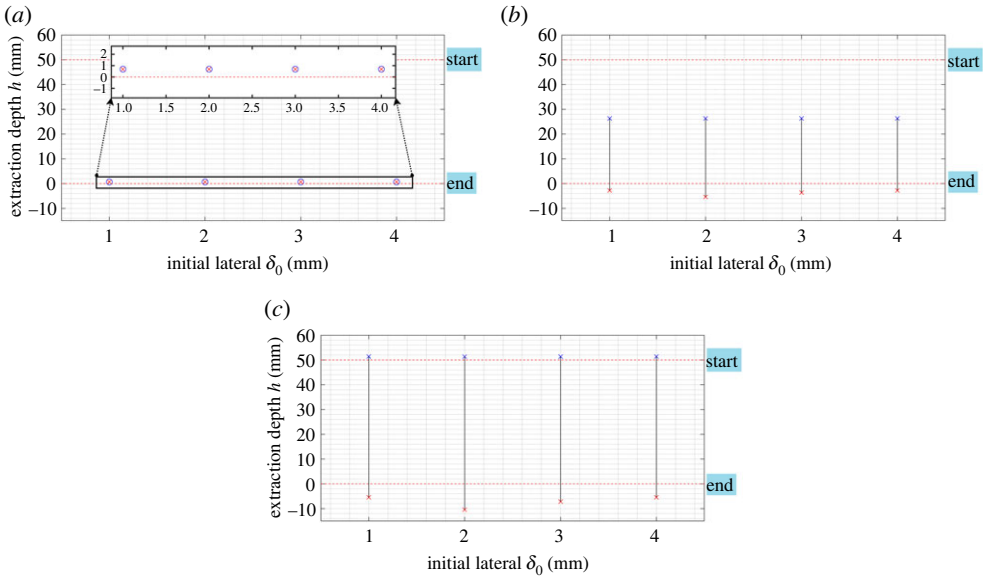

Figure 14. The effect of initial lateral error on the two-point contact region in the contact of the external surfaces of the pegs with the holes: (*a*) $L_C = 0$, (*b*) $L_C = 25$, (*c*) $L_C = 50$ with $\beta_0 = 0$ rad, $K_\theta = 4$ N mm^{-1}, $K_\theta = 30$ Nmm rad^{-1}.

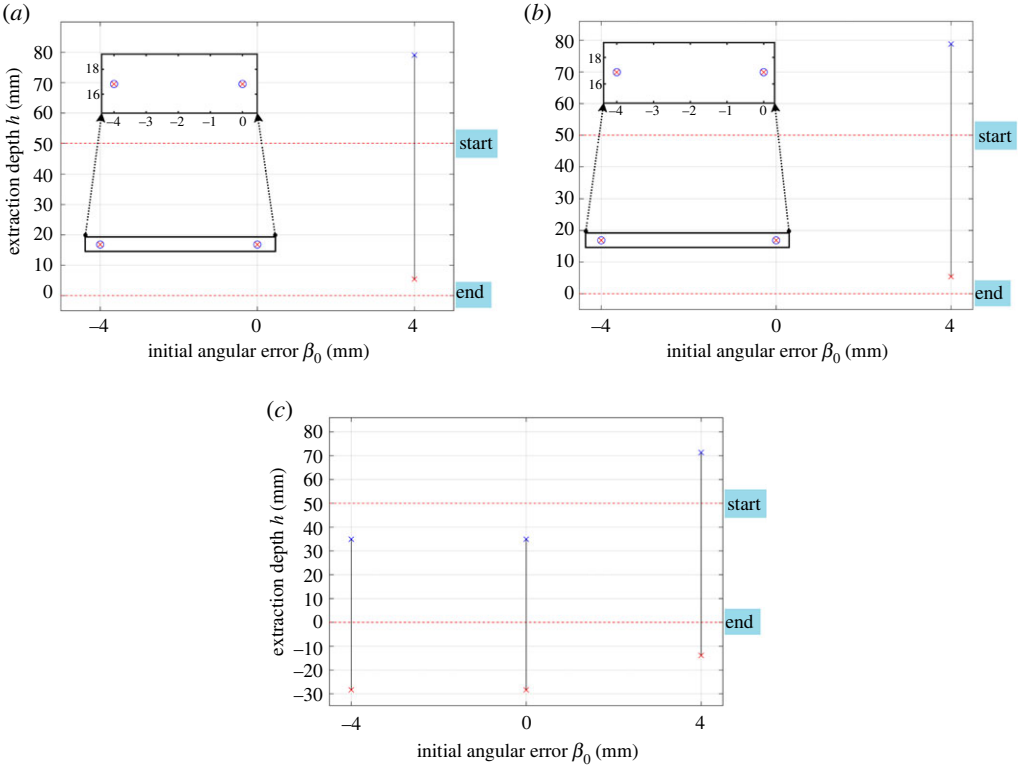

Figure 15. Dependence of the two-point contact region on the initial angular error: with $L_C = 50$ mm, $\delta_0 = 1$ mm, rad, $K_x = 4$ N mm^{-1} and $K_\theta = 30$ Nmm rad^{-1}. (*a*) Contact in one of the dual peg-holes, (*b*) external surfaces of pegs contact hole surfaces, (*c*) inner surfaces of pegs contact hole surfaces.

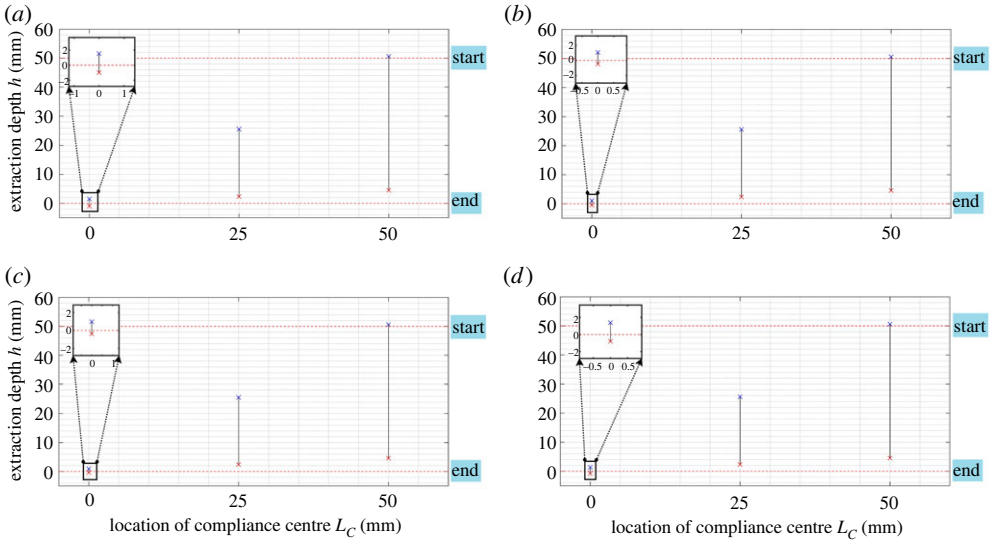

Figure 16. The effect of the two-point contact region in one of the dual peg-holes on the structural parameters: (*a*) $K_x = 2$ N mm^{-1}, $K_\theta = 30$ Nmm rad^{-1}; (*b*) $K_x = 6$ N mm^{-1}, $K_\theta = 30$ Nmm rad^{-1}; (*c*) $K_x = 4$ N mm^{-1}, $K_\theta = 15$ Nmm rad^{-1}; (*d*) $K_x = 4$ N mm^{-1}, $K_\theta = 45$ Nmm rad^{-1} with $\delta_0 = 2$ mm, $\beta_0 = 0$ rad.

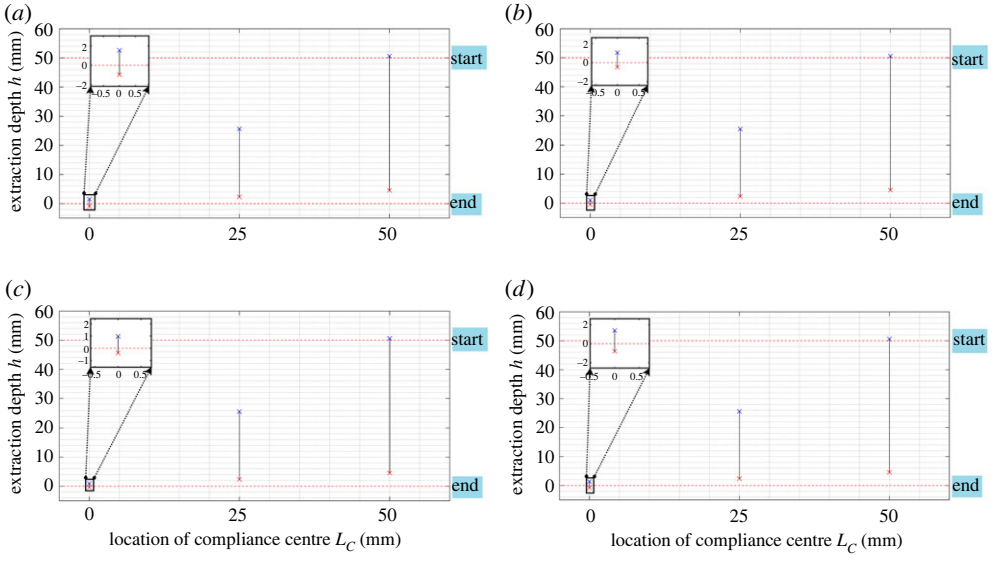

Figure 17. The effect of the two-point contact region in the contact of the inner surfaces of the pegs with the holes on the structural parameters: (*a*), $K_x = 2$ N mm^{-1}, $K_\theta = 30$ N mm rad^{-1}; (*b*), $K_x = 6$ N mm^{-1}, $K_\theta = 30$ Nmm rad^{-1}; (*c*), $K_x = 4$ N mm^{-1}, $K_\theta = 15$ Nmm rad^{-1}; (*d*), $K_x = 4$ N mm^{-1}, $K_\theta = 45$ Nmm rad^{-1} with $\delta_0 = 2$ mm, $\beta_0 = 0$ rad.

(iii) Stiffness

A successful disassembly task depends on the location of the compliance centre on the peg and the coupling stiffness element between the translational and rotational directions [6]. Compliant manipulators define lateral and angular compliance based on their rotational and lateral stiffnesses. Figures 16–18*a*,*b* show that as the lateral stiffness and location of the centre

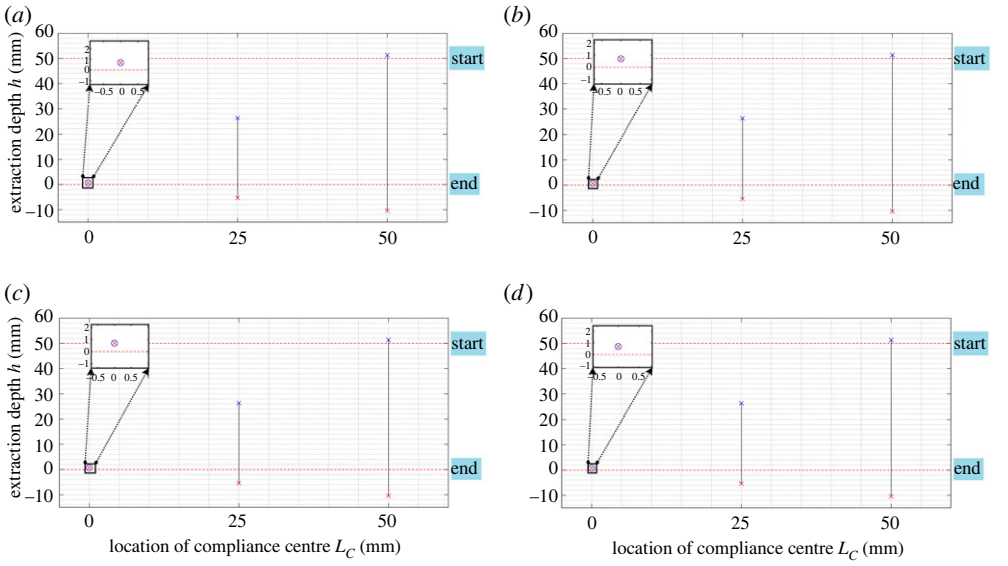

Figure 18. The effect of the two-point contact region in the contact of the external surfaces of the pegs with the holes on the structural parameters: (*a*), $K_x = 2$ N mm^{-1}, $K_\theta = 30$ Nmm rad^{-1}; (*b*), $K_x = 6$ N mm^{-1}, $K_\theta = 30$ Nmm rad^{-1}; (*c*), $K_x = 4$ N mm^{-1}, $K_\theta = 15$ Nmm rad^{-1}; (*d*), $K_x = 4$ N mm^{-1}, $K_\theta = 45$ Nmm rad^{-1} with $\delta_0 = 2$ mm, $\beta_0 = 0$ rad.

Table 2. Parameters for dual peg-hole.

category	parameter	value
friction characteristics	coefficient of friction	$\mu = 0.01$
geometrical parameters	Pegs mass	$m = 0.6$ kg
	Pegs radius	$r = 5.7$, 6 and 6.5 mm
	Holes radius	$R = 6.1$ mm
	Pegs length	$L = 50$ mm
	distance between two centres of pegs/holes	$D = 40$ mm
	clearance ratio	$C = 0.01639, 0.06557, 0.00819$
initial position/angle	depth	$h_0 = 50$ mm
	angle	$\theta_0 = -0.9$ rad

of compliance increase, the two-point contact region decreases. This is because increased lateral stiffness causes the pegs to rotate less for similar positional errors, reducing the two-point contact region.

The two-point contact region, on the other hand, increases with increasing angular stiffness regardless of the location of the compliance centre (figures 16–18*c*,*d*). According to these figures, stiffness does not significantly influence the two-point contact region.

5. Experiment

In this section, an experiment is performed with three samples with different radii to verify the results of the above analysis. Dual peg-holes have the following geometric dimensions (table 2).

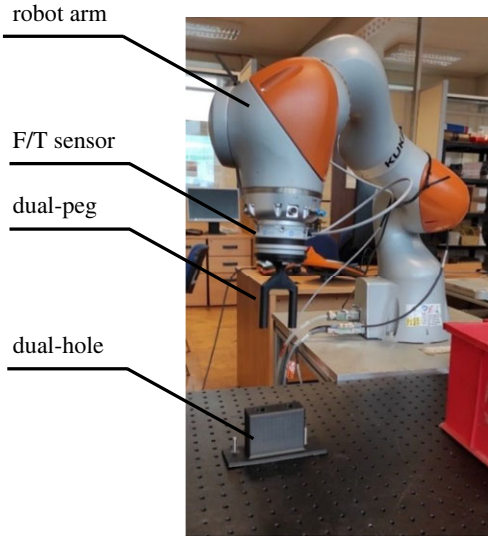

Figure 19. The experimental equipment.

(a) Experimental design

The experiment presented in this section uses a 6 d.f. KUKA LBR iiwa robot [29] and a force/torque sensor (figure 19). The experimental video can be found at [30]. In this experiment, the force and moment were sampled accordingly. The hole block was positioned on a table while the peg was attached to the media flange of a robot arm.

The exclusion of a gripper in this setup facilitates the examination of the compliance centre's impact. It is noteworthy that established literature, including Zhang *et al*'s work [12], frequently uses the approach of affixing the workpiece to the robot's end effector.

The peg and hole were made of thermoplastic material. The experiment was repeated 18 times for each sample, with six repetitions for each compliance centre location ($L_C = 50$ mm, $L_C = 25$ mm and $L_C = 0$ mm).

The tool centre point (TCP) was also created using active compliance. In this experiment, the peg could rotate around the TCP without changing its position. To simulate the different locations of the compliance centre, several TCPs were configured. Lateral and angular stiffness could also be controlled [29].

(b) Experimental results

The experimental parameters are listed in table 2. Along the extraction direction, a stiffness of $K_x = 3\,\mathrm{N\,mm^{-1}}$ is set. A Savitzky–Golay filter was used to remove noise before plotting extraction force measurements. Figure 20 shows the effects of the compliance centre location on extraction forces with depth or three samples with different radii. The area of two-point contact increases with increasing extraction force. It is evident that both in theory and practice, the contact states significantly differ based on the position of the compliance centre. The blue curve shows that when the compliance centre was far from the tip of the dual-peg, the two-point contact region was the largest. The orange and green curves show narrower and lower peaks when L_C decreases, corresponding to a smaller two-point contact region.

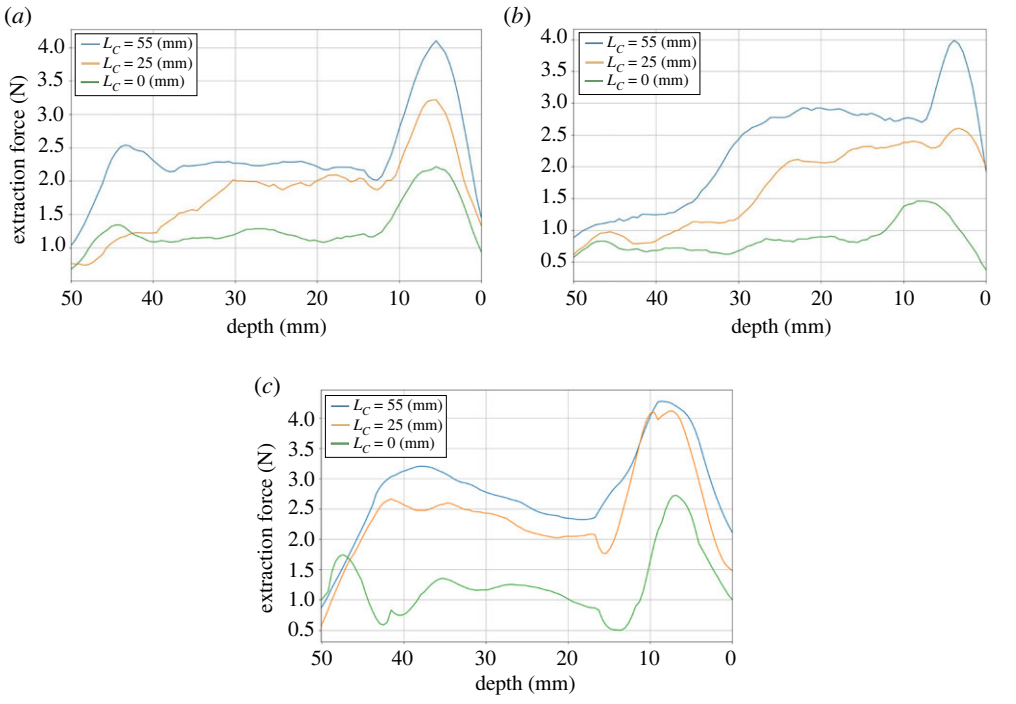

Figure 20. Extraction force curves based on compliance centre locations. (*a*) $r = 5.7$ mm, (*b*) $r = 6$ mm and (*c*) $r = 6.5$ mm.

6. Conclusion

This paper presents a geometric and static force analysis for the dual-peg extraction jamming problem, considering all geometric variations. In a dual peg jamming problem, all 13 contact states are identified.

The applied geometric and quasi-static force analysis approach proves effective in studying the jamming phenomenon and exhibits potential for application to other assembly and disassembly problems.

The incorporation of compliant manipulators offers the opportunity to establish geometric and force/moment conditions for each contact state, underscoring the potential for developing more precise and reliable robotic systems tailored for disassembly and remanufacturing tasks. In this investigation, we delve into several factors, including the location of the compliance centre, initial lateral and angular errors, and manipulator stiffness, to assess their influence on the area of the two-point contact. Of particular note, our results emphasize the pivotal role played by the location of the compliance centre.

Our theoretical exploration demonstrates striking similarities between the dual peg-hole extraction process and its single peg-hole counterpart. This suggests that techniques developed for single peg-hole scenarios, such as the compliance centre approach, can be viably applied to the dual peg-hole case as well, providing an effective strategy.

To corroborate our theoretical findings, we conducted experiments. Our research confirms that the application of appropriate compliance strategies, such as adjusting stiffness and the remote centre of compliance, can significantly reduce disassembly forces. While it is true that the jamming conditions differ between single and dual peg-holes, as illustrated in figure 12, with 13 contact states compared to the three contact states in a single peg-hole [12], the judicious use of remote compliance strategies proves effective in mitigating disassembly forces in both scenarios. The experimental outcomes align with the predictions of the theoretical model concerning the disassembly of dual-peg-hole assemblies, further reinforcing the credibility and reliability of the study's findings.

Data accessibility. All data sources are available as part of the electronic supplementary material [31]. This ensures that the data associated with the study can be readily accessed for reference, transparency and reproducibility.
Declaration of AI use. We have not used AI-assisted technologies in creating this article.
Authors' contributions. F.G.: formal analysis, investigation, methodology, project administration, software, writing—original draft; Y.Z.: formal analysis, methodology, writing—review and editing; M.Q.: investigation, software, writing—review and editing; Y.Z.: investigation, writing—review and editing; M.S.: supervision, writing—review and editing; D.T.P.: conceptualization, writing—review and editing; Y.W.: conceptualization, project administration, resources, supervision, writing—review and editing.

All authors gave final approval for publication and agreed to be held accountable for the work performed therein.

Conflict of interest declaration. We declare we have no competing interests.
Funding. This work was supported by the Engineering and Physical Sciences Research Council (EPSRC) under grant no. EP/W00206X/1.

Appendix A

variable	description	formula	state no
C	clearance ratio	$C = (R - r)/R$	
D	diameter of the hole (mm)	camera	
F_x	lateral force (N)	$F_X = -K_x\left(\delta_0 + L_C\theta_0 - \frac{CDL_C}{h}\right)$	5
		$F_x = -k_x\left(\delta_0 - \varepsilon_0 + L_C\theta_0 + \frac{cD}{2} - \frac{cDL_c}{h}\right)$	10
		$F_x = -k_x\left(\delta_0 + L_C\theta_0 - \frac{L_C(-2R'C)}{h}\right)$	9
F_{fr1}	friction force at contact point 1 (N)		
F_{fr2}	friction force at contact point 2 (N)		
F_{N1}	reaction force at contact point 1 (N)		
F_{N2}	reaction force at contact point 2 (N)		
F_z	extraction force (N)	$F_z = \frac{M}{\lambda r} - \frac{\mu}{\lambda}(1-\lambda)F_x, \quad \lambda = \frac{h}{(2r\mu)}$	
F_z one-point contact	extraction force (N)	$F_z = \frac{\mu k_\theta(\theta - \theta_0 + \beta_0)}{(h - \mu r - L_c)}$	
h	extraction depth (mm)	$h = \frac{(2R - 2r\cos\theta)}{\sin\theta}$	
h_0	initial depth of the peg in the hole (mm)	$h_0 = \frac{(2R - 2r\cos\theta_0)}{\sin\theta_0}$	
H	height of each peg (mm)		
K_x	lateral stiffness of the compliant manipulator (N mm^{-1})		
K_z	vertical stiffness of the compliant manipulator (N mm^{-1})		
K_θ	rotational stiffness of the compliant manipulator (N mm rad^{-1})		
L_C	location of the compliance centre (mm)		
M	moment applied on the peg (Nmm)		
r	radius of each peg (mm)	camera	
R	radius of each hole (mm)	$R = D/2$	
$2R'$	distance between two holes (mm)	Camera	
$2r'$	distance between two pegs (mm)	Camera	

(*Continued.*)

variable	description		state no
U_0	initial distance between the compliance centre and the hole axis (mm)	$\lvert X_{\text{hole}} - X_C \rvert$	
U	distance between the compliance centre and the hole axis (mm)	$U = U_0 + \delta_0 - \frac{K_\theta(L_C\beta_0+\delta_0)}{K_xL_C(h-\mu r)-K_xL_C^2+K_\theta}$	5
		$U = U_0 + \delta_0 - \frac{K_\theta(L_C\beta_0+\delta_0+cR-\varepsilon_0)}{K_xL_C(h-\mu r)-K_xL_C^2+K_\theta}$	10
		$U = U_0 + \delta_0 - \frac{K_\theta(L_C\beta_0+\delta_0)}{K_xL_C(h-\mu R')-K_xL_C^2+K_\theta}$	9
β_0	initial angular error (rad)		
δ_0	initial lateral error (mm)		
ε	distance between the selected peg tip and the hole axis (mm)		
ε_0	initial distance between the selected peg tip and the hole axis (mm)	$\varepsilon_0 = L_C \sin\theta_0 - U_0$	
θ	tilt of the peg (rad)	$\theta = \theta_0 - \beta_0 + \frac{K_x(h-\mu r-L_C)(L_C\beta_0+\delta_0)}{K_xL_C(h-\mu r)-K_xL_C^2+K_\theta}$	5
		$\theta = \theta_0 - \beta_0 + \frac{K_x(h-\mu r-L_C)(L_C\beta_0+\delta_0+cR-\varepsilon_0)}{K_xL_C(h-\mu r)-K_xL_C^2+K_\theta}$	10
θ_0	initial tilt angle of the peg (rad)	$\theta = \theta_0 - \beta_0 + \frac{K_x(h-\mu R'-L_C)(\delta_0+L_C\beta_0)}{K_xL_C(h-\mu R')-K_xL_C^2+K_\theta}$	9
μ	coefficient of friction		

References

1. Goli F, Wang Y, Saadat M. 2022 Perspective of self-learning robotics for disassembly automation. *In* 2022 27th International Conference on Automation and Computing (ICAC). Bristol, UK, 1-3 Sep 2022, pp. 1–6. New York, NY: IEEE. (doi:10.1109/ICAC55051.2022.9911085)
2. Mule JY. 2012 Design for Disassembly Approaches on Product Development. *IJSER* **3**, 1–5.
3. Ijomah WL, McMahon CA, Hammond GP, Newman ST. 2007 Development of robust design-for-remanufacturing guidelines to further the aims of sustainable development. *Int. J. Prod. Res.* **45**, 4513–4536. (doi:10.1080/00207540701450138)
4. Vongbunyong S, Chen WH. 2015 Disassembly automation. In *Disassembly Automation: Automated Systems with Cognitive Abilities* (eds S Vongbunyong, WH Chen), pp. 25–54. Cham: Springer International Publishing. (doi:10.1007/978-3-319-15183-0)
5. Tang Y, Zhou M, Zussman E, Caudill R. 2002 Disassembly modeling, planning, and application. *J. Manuf. Syst.* **21**, 200–217. (doi:10.1016/S0278-6125(02)80162-5)
6. Kim BH, Yi BJ, Suh IH, Oh SR. 2000 Stiffness analysis for effective peg-in/out-hole tasks using multi-fingered robot hands. In *Proc. 2000 IEEE/RSJ Int. Conf. on Intelligent Robots and Systems (IROS 2000) (Cat No00CH37113)*, vol. 2, Takamatsu, Japan 31 October - 5 November 2000, pp. 1229–1236. New York, NY: IEEE. (doi: 10.1109/IROS.2000.893187)
7. James B, Rao P, Reddy E, Mallikarjuna V. 2016 Design and analysis of turbochargers. *Int. J. Eng. Res.* **4**, 302–312.
8. Bdiwi M, Rashid A, Pfeifer M, Putz M. 2017 Disassembly of unknown models of electrical vehicle motors using innovative human robot cooperation. pp. 85–86.
9. Usubamatov R, Leong KW. 2011 Analyses of peg-hole jamming in automatic assembly machines. *Assem. Autom.* **31**, 358–362. (doi:10.1108/01445151111172943)
10. Whitney DE. 1982 Quasi-static assembly of compliantly supported rigid parts. *J. Dyn. Syst. Meas. Control.* **104**, 65–77. (doi:10.1115/1.3149634)
11. McNelly BP, Leary R, Brennan S, Reichard K. 2016 Characterizing successful robotic insertion and removal from a dry storage cask using peg-like jamming and wedging analysis. In *Pressure Vessels and Piping Conference*. Vancouver, Canada, 17-21 July 2016. New York, NY: ASME. (doi:10.1115/PVP2016-63634)

12. Zhang Y, Lu H, Pham DT, Wang Y, Qu M, Lim J, Su S. 2019 Peg–hole disassembly using active compliance. *R. Soc. Open Sci.* **6**, 190476. (doi:10.1098/rsos.190476)
13. Asada H, Kakumoto Y. 1988 The dynamic RCC hand for high-speed assembly. In *Proc. 1988 IEEE Int. Conf. on Robotics and Automation*, vol. 1. Philadelphia, PA, 24-29 April 1988, pp. 120–125. New York, NY: IEEE. (doi:10.1109/ROBOT.1988.12035)
14. SimunoviSN. 1979 *An Information Approach to Parts Mating*. Cambridge, MA: Massachusetts Institute of Technology.
15. Nevins JL, Whitney DE. 1979 Assembly research. *IFAC Proc.* **12**, 195–214. (doi:10.1016/S1474-6670(17)65359-X)
16. Caine ME, Lozano-Perez T, Seering WP. 1989 Assembly strategies for chamferless parts. In *Proc. 1989 Int. Conf. on Robotics and Automation*, vol. 1. Scottsdale, AZ, 14-19 May 1989, pp. 472–477. New York, NY: IEEE. (doi:10.1109/ROBOT.1989.100031)
17. Sturges RH. 1988 A three-dimensional assembly task quantification with application to machine dexterity. *Int. J. Rob. Res.* **7**, 34–78. (doi:10.1177/027836498800700403)
18. Sturges Jr RH, Laowattana S. 1996 Virtual wedging in three-dimensional peg insertion tasks. *J. Mech. Des.* **118**, 99–105. (doi:10.1115/1.2826863)
19. Sturges Jr RH, Laowattana S. 1996 Design of an orthogonal compliance for polygonal peg insertion. *J. Mech. Des.* **118**, 106–114. (doi:10.1115/1.2826840)
20. Strip DR. 1988 Insertions using geometric analysis and hybrid force-position control: method and analysis. In Proc. 1988 IEEE Int. Conf. on Robotics and Automation, pp. 1744–1751. IEEE.
21. Wang W, Loh RNK, Gu EY. 1998 Passive compliance versus active compliance in robot-based automated assembly systems. *Ind. Robot: An Int.l J.* **25**, 48–57. (doi:10.1108/01439919810196964)
22. Zhang X, Zheng Y, Ota J, Huang Y. 2017 Peg-in-hole assembly based on two-phase scheme and f/t sensor for dual-arm robot. *Sensors* **17**, 2004. (doi:10.3390/s17092004)
23. Sathirakul K, Sturges RH. 1998 Jamming conditions for multiple peg-in-hole assemblies. *Robotica* **16**, 329–345. (doi:10.1017/S0263574798000393)
24. Fei Y, Zhao X. 2003 An assembly process modeling and analysis for robotic multiple peg-in-hole. *J. Intell. Robot Syst.* **36**, 175–189. (doi:10.1023/A:1022698606139)
25. Lan F, Castellani M, Truong Pham D, Wang Y. 2023 On the correctness of using two-dimensional representations in the analysis of cylindrical peg–hole insertion and withdrawal. *R. Soc. Open Sci.* **10**, 221021. (doi:10.1098/rsos.221021)
26. Wang S, Chen G, Xu H, Wang Z. 2019 A robotic peg-in-hole assembly strategy based on variable compliance center. *IEEE Access* **7**, 167 534–167 546. (doi:10.1109/ACCESS.2019.2954459)
27. Fei Y, Zhao X. 2005 Jamming analyses for dual peg-in-hole insertions in three dimensions. *Robotica* **23**, 83–91. (doi:10.1017/S0263574704000578)
28. Trong DN, Betemps M, Jutard A. 1995 Analysis of dynamic assembly using passive compliance. In *Proc. of 1995 IEEE Int. Conf. on Robotics and Automation*, vol. 2. Nagoya, Japan, 21-27 May 1995, pp. 1997–2002. New York, NY: IEEE. (doi:10.1109/ROBOT.1995.525556)
29. 2016 System Software KUKA Sunrise.OS 1.11 KUKA Sunrise. Workbench 1.11 Operating and Programming Instructions for System Integrators.
30. Goli F. 2023 Dual peg-hole disassembly process with active compliance centre [Internet]. See https://youtube.com/shorts/hDh6vXg1V.
31. Goli F, Zhang Y, Qu M, Zang Y, Saadat M, Pham DT, Wang Y. 2024 Jamming problems and the effects of compliance in dual peg-hole disassembly. Figshare. (https://figshare.com/s/9a9df1ea0a0a4c535aa7)